Exploring surface science and restructuring in reactive atmospheres of colloidally prepared bimetallic CuNi and CuCo nanoparticles on SiO_2 *in situ* using ambient pressure X-ray photoelectron spectroscopy

Simon K. Beaumont, [a‡] Selim Alayoglu,[a] Vladimir V. Pushkarev,[a] Zhi Liu,[c] Norbert Kruse[d] and Gabor A. Somorjai[a,b]*

DOI: 10.1039/b000000x

Bimetallic nanoparticles (~11 nm diameter) of CuNi and CuCo were prepared by a new synthetic route and the 1:1 atomic ratio of their constituent elements confirmed using STEM-EDS at a single particle level. These nanoparticles, supported on the native oxide layer of a silicon wafer, were studied *in situ* in a series of reactive gas atmospheres ($H_2 \rightarrow CO$ or $CO/H_2 \rightarrow O_2 \rightarrow H_2$) using ambient pressure x-ray photoelectron spectroscopy (AP-XPS). Despite the deliberate similarity of nickel and cobalt with respect to copper, their restructuring behaviour is different. CuNi nanoparticles were found to surface segregate nickel in H_2, but copper in O_2 reversibly, while CuCo nanoparticles were found to surface segregate copper irreversibly when exposed to O_2, such that the surface remains copper rich when re-exposed to H_2. Both systems also restructure in opposition the behaviour predicted by the surface free energies and enthalpies of oxide formation of the elements from which they are comprised – factors that are seen to control restructuring and surface segregation in many similar systems.

Introduction

Bimetallic heterogeneous catalysts have long been known to exhibit interesting or useful properties not found in their individual constituent metals. For this reason, they find extensive use in many important chemical processes. Obvious examples include the use of bimetallic catalysts containing either Pt or Pd for isomerisation, olefin hydrogenation and alcohol synthesis, or PtSn in hydrocarbon reforming and dehydrogenation reactions.[1] Increasingly, there are numerous reports in the literature of new bimetallic combinations being used as heterogeneous catalysts for a large variety of chemical transformations. A current example of this is the pressure to develop or improve catalytic transformations to tackle dwindling fossil fuel reserves - this has led to a huge interest in syngas conversion chemistry. In this field many bimetallic systems have been considered,[2] but also some very systematic theoretical efforts have been employed to consider all plausible combinations of bimetallic surfaces.[3] Another merit of bimetallics has been the possibility of lowering cost while maintaining performance through the use of a precious metal in combination with a more abundant, cheaper metal, the properties of the former still being retained. An example of this is the suggested use of Pt skin – Ni core nanoparticles

as PEM fuel cell catalysts.[4]

Early research in the use of heterogeneous bimetallic catalysts began by developing the well known theories of 'ensemble' *vs.* 'electronic' effect,[5] often responsible for the enhanced properties conferred upon a catalyst by surface alloying. The advent of ultra high vacuum science in the latter half of the 20th century allowed surface systems to be studied in detail and much work was done to explore and understand the surface segregation of metals.[6] For bulk materials their behaviours in vacuum can be understood as a thermodynamic competition of entropy, cohesive and surface energies.[7] Lattice strain and relaxation effects were generally considered too small to be important.[6] In the present paper we focus on exploring the changes on going from a bulk material to bimetallic metal nanoparticles, of which heterogeneous catalysts are normally comprised. This changes a number of important factors by essentially diminishing the importance of bulk energy terms relative to surface energy terms on the thermodynamic equilibrium structure of the particle. These are likely to include:

- The greater importance of surface free energy (It is also noteworthy that the surface energy itself will be particle size dependant,[8] as has been shown experimentally for PtRh nanoparticles.[9])
- Surface-adsorbate interactions becoming a significant energetic term when balanced by very little 'bulk.' Furthermore, surface oxide or hydride formation a few atomic layers deep may account for a large fraction of the particle (as there are many more surface atoms) and thus be a major energetic term.
- Diminished importance of kinetic limitations; in many bulk systems it is valid to assume only the top layer or layers of an alloy are restructured at moderate temperature,[6] whereas for nanoparticles complete restructuring of the material to reach thermodynamic equilibrium has been seen on the 15 minute timescale of an ambient pressure XPS experiment.[10]
- Entropy of mixing is less important as partial surface segregation represents a much higher fraction of the possible configurations available to the atoms within the nanoparticle (in contrast to a bulk material where entropy strongly promotes mixing into the bulk).
- The low co-ordination of many surface sites means relaxation and strain effects can be expected to also differ from those in a bulk material, as seen for RuPt core-shell nanoparticles.[11]

The first two of these points concerning the increased importance of surface energy and adsorbate-surface interactions are particularly significant in catalysis, where very reactive, high pressure gases (or liquids) are usually present. In 2004 Lang *et al*. reported apparently anomalous results in the infrared characterisation of AuPt clusters on SiO_2, using CO as a probe molecule.[12] They observed the Au signal decrease and the Pt signal grow under exposure to CO at moderate temperature (140 °C). This was attributed to surface segregation resulting from the strong interaction of Pt with CO (while Au has the lower surface free energy in vacuum).

As indicated in Table 1, in the last decade the phenomena of bimetallic nanoparticle restructuring has been the focus of considerable work by our group and others, in particular utilising new *in situ* techniques, such as ambient pressure XPS. Indeed, bimetallic nanoparticle catalysts have been the focus of a variety of *in situ* studies and the details of these are well reviewed elsewhere.[13] The ambient pressure XPS technique is particularly powerful for addressing the question of how and when nanoparticles undergo restructuring. It enables element and oxidation state specific

information to be collected in the 0.1 – 10 torr range – where there are already ~ 10^6 collisions per second per surface atom making mass transfer of adsorbates in the gas phase prior to adsorption cease to be rate limiting in most cases.[14] This technique, described elsewhere,[15] circumvents the usual limitation that emitted photoelectrons have too short a mean free path in ambient gas to be measured. This is achieved by bringing a small, differentially pumped aperture cone very close to the sample surface. This allows gas pressure at the sample to be maintained, while photoelectrons emitted from the sample quickly escape through the aperture to near vacuum conditions, enabling them to be collected and analysed. In combination with synchrotron radiation, AP-XPS is especially powerful, allowing highly surface sensitive measurements and depth profiling by varying the incident photon energy.[16] (This utilises the fact the incident photon energy can be tuned to limit the possible mean free path of photoelectrons produced from a given core level, thus controlling the depth from within the sample that the spectra obtained represent.)[17]

Table 1: Reported bimetallic nanoparticles systems studied under reactive gas conditions and the resulting structural effects observed. ([a]NO+CO is reducing.)

System studied	Technique used	Conditions and segregation effect		Factors controlling structure
AuCu[18]	*in situ* XANES	500 °C H_2 Cu migrates to core	3-400 °C O_2/CO CuO_x surface patches	n/a
AuPd[19]	*in situ* XAFS, PDF & DRIFTS	Vac; RT No surface enrichment	350 °C CO Pd rich surface	CO-Pd bond formation
AuPd[20]	AP-XPS	Vac; RT Pd rich surface	200 °C O_2/CO Au-rich particles, restructure to Au surfaces, others remain Pd rich	surface/ cohesive energy; adsorption enthalpies
AuPt[12]	infrared of CO stretching	Vac; RT Au migrates to surface	140 °C CO Pt enriched on surface	workfunction *vs.* M-CO bond
SnPt[21]	*in situ* XAFS/QXAFS	400 °C O_2 SnO_2 on surface	400 °C H_2 Returns to Pt_3Sn	structural oxidation
PtRh[10]	AP-XPS	300 °C NO Rh surface segregation	300 °C H_2 Pt enriched surface	ΔH°_f(oxide) vs. surface free energy
PdRh[22,10]	AP-XPS	300 °C NO Rh surface segregation	300 °C NO+CO[a] or H_2 Pd surface segregation	Rh oxide formation
PtPd[10,22]	AP-XPS	300 °C NO Pd remains on surface	300 °C NO+CO[a] or H_2 Pd remains on surface	ΔH°_f(oxide) vs. surface free energy
PtCu[19]	in situ XAFS, PDF & DRIFTS	Vac; RT Cu rich surface	350 °C CO Pt rich surface	CO - Pt surface adsorption
PtCo[23]	electro-chemistry	200 °C CO Pt surface segregation		segregation *vs* surface mixing; Pt-CO *vs* Co-CO
PtCo[24]	AP-XPS, *in situ* NEXAFS	247 °C O_2 Co enriched at surface	247 °C H_2 Pt segregates to surface	kinetically controlled
PtCo[25]	AP-XPS & ETEM	Vac; RT Both metals on surface	250 °C in H_2 Pt forms surface shell	n/a
PtCo[26]	AP-XPS, *in situ* NEXAFS	125 °C H_2 Pt surface segregation	125 °C in CO/O_2 Co segregates to surface, not oxidised	adsorbate induced restructuring
AgCu[27]	AP-XPS	247 ° O_2 & O_2/C_2H_4 Cu enriched at surface	247 °C H_2 Less Cu at surface	surface energies and CuO formation

Table 1 illustrates many examples in which oxidation or formation of surface oxides is suggested to be the dominant factor in their restructuring. This has either been for systems such as PtRh where neither has a strong propensity to form oxides (it is their relative difference) or for systems such as PtCo where the size mismatch of the atoms is very large and may be contributory to restructuring effects. All these examples involve at least one heavy element (4d or 5d) and to our knowledge these types of studies haven't been conducted on any combinations of 3d metals. These have much higher propensities to form oxides and very similar sizes. Owing to their abundance, and thus lower cost, they are also a very common choice as possible elements to involve in forming new bimetallic catalysts. Accordingly, we have chosen to consider Cu in combination with Co and Ni. These three all have similar metallic radii (128, 125 and 125 pm respectively) and much greater enthalpies of oxide formation per metal atom than the precious metals studied previously.[28]

Here, CuCo and CuNi nanoparticles of 1:1 atomic composition of the two metals and of similar sizes (~11 nm) were prepared using a new colloidal synthesis. These have then been supported on a planar SiO_2 surface and characterised in oxidising and reducing environments using ambient pressure XPS. With this new data, we aim to inform a discussion of how such bimetallic nanoparticles behave under catalytic conditions and the importance of addressing this issue experimentally and theoretically in the preparation of new heterogeneous bimetallic catalysts.

Experimental Methods

A Synthesis of $Cu_{50}Co_{50}$ and $Cu_{50}Ni_{50}$ nanoparticles

All chemicals were used as obtained from the supplier. $Ni(acac)_2$ was stored in darkness.

11 nm $Cu_{50}Co_{50}$ nanoparticles: The metal precursor salts were dissolved in a reducing, coordinating solvent (oleylamine) at 80 °C. Typically, $Cu(acac)_2$ (27.1 mg, Aldrich, ≥99.99% pure) and $Co(acac)_2$ (26.7 mg, Aldrich, ≥99.0% pure) were dissolved in oleylamine (5 mL) in a 50 mL round bottom flask. The flask was evacuated and subsequently flushed with Ar. The evacuation/purging cycle was repeated several times before the solution was purged by bubbling Ar through it for 15 minutes. Finally, the reaction flask was submerged in an oil bath preheated to 230 °C. The solution turned black, indicating the formation of colloidal particles after approximately 2 minutes. This colloidal suspension was then aged at 230 °C for 10 minutes prior to terminating the reaction by rapid cooling by removing it from the oil bath. After reaching room temperature the nanoparticles were precipitated from the colloidal solution with acetone, centrifuged and re-dispersed in toluene. As synthesized nanoparticles were then stored in toluene until further use.

11 nm $Cu_{50}Ni_{50}$ nanoparticles: The synthetic procedure was identical to that of the $Cu_{50}Co_{50}$ nanoparticles, except that $Ni(acac)_2$ (27.3 mg, Aldrich, 95.0% pure) was used in place of $Co(acac)_2$.

B Ambient pressure XPS

AP-XPS experiments were conducted at Beamline 9.3.2 at the Advanced Light Source, Lawrence Berkeley National Laboratory. Samples were prepared as dipcoat films of nanoparticles to yield 2D films on 275 μm thick Si wafers. The choice of Si wafers to anchor the nanoparticles to was selected to mimic a typical heterogeneous

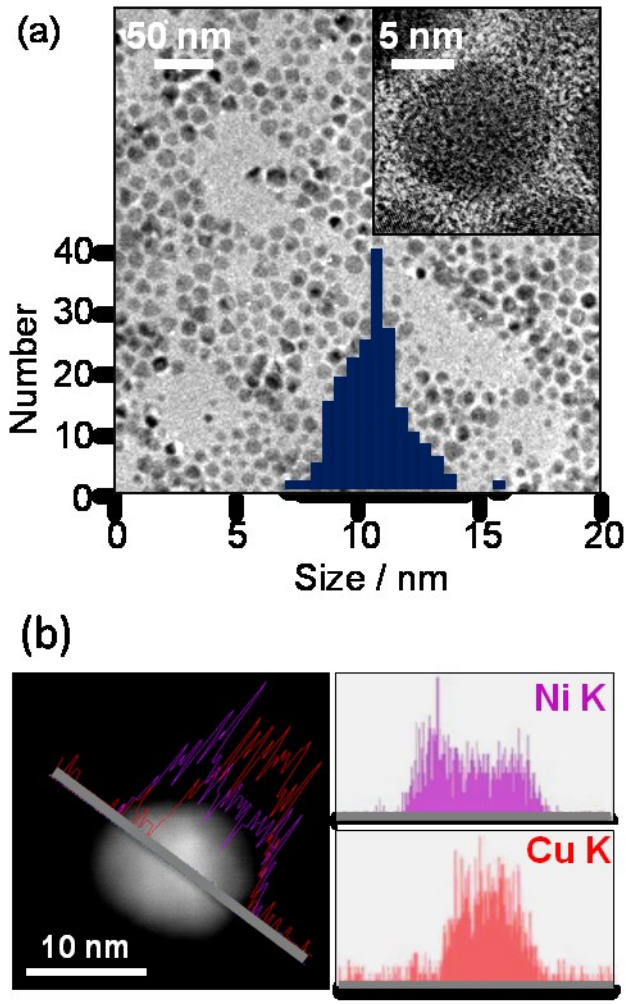

Fig. 1 (a) Representative HR-TEM images of the as prepared CuNi nanoparticles, with the sample size distribution obtained by counting a large number of nanoparticles from different regions of the TEM grid superimposed above the image. (b) High Angle Annular Dark Field (HAADF) image of a CuNi nanoparticle, the grey line indicating the line along which scanning TEM (STEM) linescans using Energy Dispersive X-ray Spectra (EDS) were acquired for Cu K and Ni K edges as shown on right.

catalyst oxide support and avoid any risk of alloying with a gold surface, often used as the support when preparing 2-D films of nanoparticles. Ambient Pressure XPS was conducted using an apparatus described elsewhere.[29] The instrument also takes advantage of the tunable incident photon energy of synchrotron-generated X-rays to enable acquisition of both very surface sensitive measurements as well as near-surface depth profiles of both oxidation state and elemental composition of the samples. Owing to the range of accessible energies with this instrument, spectra were collected using electrons excited from the Cu 3p, Co 3p and Ni 3p levels (rather than the 2p levels usually used in a conventional laboratory XPS when using an Al Kα source). The photoionisation cross section for these elements with a 380

eV source energy is comparable to that of the 2p levels when using an Al Kα source. All energies are corrected with respect to the Fermi edge (recorded immediately prior to or following the spectrum of interest, without changing the incident photon energy). Relative concentrations in the region of the particle probed by the XPS were calculated and plotted by fitting a Shirley background using XPSPeak and then integrating. The obtained results were also corrected for the relevant photo-ionization cross sections[30] in the calculation of the relative composition of the two metals. Maximum temperatures for heating in each gas were selected based on SEM characterisation with *ex situ* thermal treatments to minimise the chance of any agglomeration occurring due to thermal activation. Probing depths are estimated using the method of Seah and Dench as described in the ESI.† The possibility of beam damage or heating causing agglomeration was examined using SEM before and after AP-XPS experiments for both samples and the results are provided in the ESI.†

C Additional Characterization

TEM and HR-TEM images, and STEM/EDS phase spectra were obtained using Jeol 2100F (scanning) transmission electron microscope. Samples were prepared by drop casting the nanoparticles (in toluene) on to an ultra thin carbon coated copper TEM grid. A Zeiss Ultra55 scanning electron microscope was then used for imaging and confirming the integrity of the dipcoated films of nanoparticles on Si wafers before and after the AP-XPS studies.

Results

CuNi bimetallic nanoparticles

Figure 1(a) shows representative TEM images of the as prepared, unsupported 10.6 ± 1.3 nm CuNi nanoparticles, prepared using an oleylamine capping agent as described above. Their corresponding size distribution is indicated above the image. Figure 1(b) shows a High Angle Annular Dark Field (HAADF) image of a nanoparticle in the same sample in which TEM (STEM) linescans using Energy Dispersive X-ray Spectra (EDS) were acquired for Cu K- and Ni K-edges as shown. These linescans confirm the presence of both metals within the individual particle and show that the as prepared particle contains a copper enriched core and a more nickel rich shell, when measured under the vacuum conditions of the TEM. (The Cu signal is strong only near the middle of the linescan, whereas the Ni is strongest at the edges, where a greater amount of the near surface region of the sphere is probed.) Additionally, this technique was used to confirm the relative metal content for 10 individual particles and it was found that they contained 53.7 ± 9.6 at. % Cu, which compares favourably to an average Cu content recorded over an area enclosing many particles of 57.2 at. % Cu. These values are also consistent with the 50 at. % Cu content targeted from the synthesis. This control over particle size and composition is crucial for enabling us to study reconstruction effects, because the spectral signals originate from a material in which all particles are near identical, rather being the average of many different systems, which would mask the effects we are seeking to probe.

The as prepared nanoparticles, supported on the silicon oxide surface of a silicon

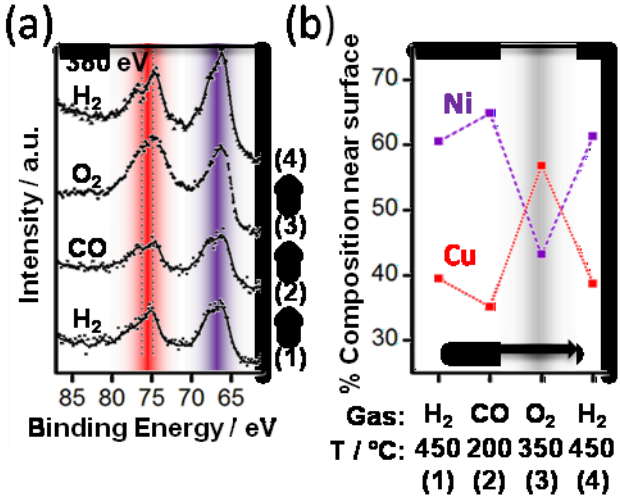

Fig. 2 (a) Ambient pressure Cu (red) and Ni (purple) 3p XP Spectra of CuNi nanoparticles supported on the native oxide layer of a silicon wafer during exposure to a series of gases as indicated (0.1 torr) using an incident photon energy of 380 eV, corresponding to a mean free path of escaping electrons of 0.8 nm. (b) Graph showing the corresponding % of Cu (red) and Ni (purple) in this top 0.8 nm surface layer of the nanoparticles for each condition in (a) (after correction for the relevant photon energy photoelectron cross sections and removal of a Shirley background).

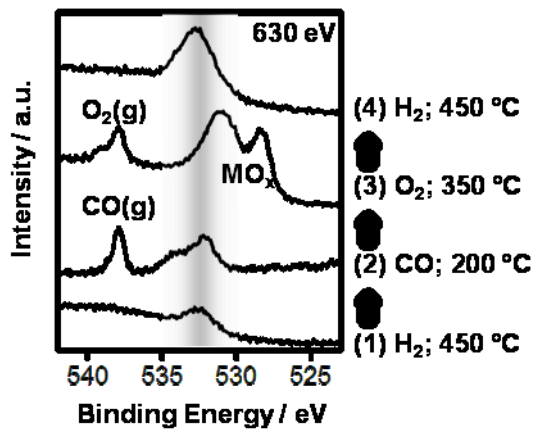

Fig. 3 Ambient pressure O 1s XP Spectra of CuNi nanoparticles supported on the native oxide layer of a silicon wafer during exposure to a series of gases as indicated (0.1 torr) using incident photon energy of 630 eV The data was acquired in the same series of numbered experiments as shown in Fig. 2.

wafer, were then investigated using ambient pressure XPS. The start-point of the XPS data is directly comparable to the TEM data above as they are both recorded on the as prepared sample, at room temperature and after evacuation in a vacuum chamber. Spectra were acquired in vacuum and during the heating steps and introduction of 100 mtorr of H_2. (See supplementary information – as these initial steps prior to heat and gas treatments are likely still dominated by the as synthesized

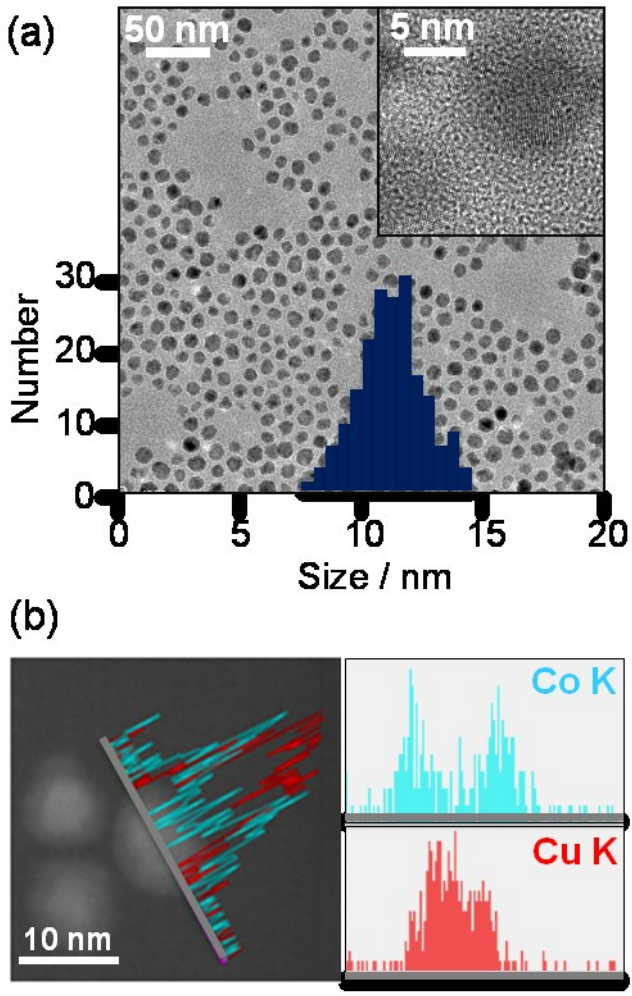

Fig. 4 (a) Representative HR-TEM images of the as prepared CuCo nanoparticles, with the sample size distribution obtained by counting a large number of nanoparticles from different regions of the TEM grid superimposed above the image. (b) High Angle Annular Dark Field (HAADF) image of CuCo nanoparticles, the grey line indicating the line along which scanning TEM (STEM) linescans using Energy Dispersive X-ray Spectra (EDS) were acquired for Cu K and Co K edges as shown on right.

structure and may not be the result of thermally activated rearrangements they will not be discussed in detail).[†] Heating in H_2 results in an enhancement of the Ni/Cu ratio in the near surface region (~ 1 nm probing depth). The major changes of interest occur on switching from reducing (H_2 or CO) to oxidising atmospheres and back again as shown in Figure 2. The spectra shown represent the top ~0.8 nm of the 10 nm diameter nanoparticles and so correspond mostly to the top 2-3 atomic layers. It is clear that nickel is dominant on the surface in H_2 (~60/40), but O_2 brings copper to the surface to produce a slightly copper rich surface. However, on re-exposure to H_2 this effect is immediately and fully reversed. In H_2 and O_2 within the accessible energy range, the sample was also probed using a higher incident photon energy

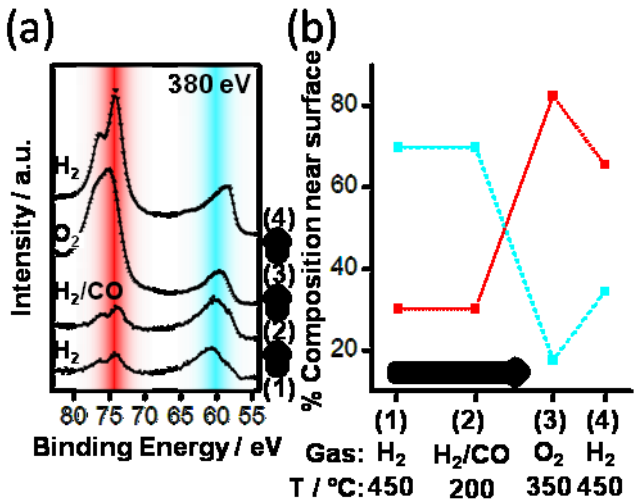

Fig. 5 (a) Ambient pressure Cu (red) and Co (blue) 3p XP Spectra of CuCo nanoparticles supported on the native oxide layer of a silicon wafer during exposure to a series of gases as indicated (0.1 torr) using an incident photon energy of 380 eV, corresponding to a mean free path of escaping electrons of 0.8 nm. (b) Graph showing the corresponding % of Cu (red) and Co (blue) in this top 0.8 nm surface layer of the nanoparticles for each condition in (a) (after correction for the relevant photon energy photoelectron cross sections and removal of a Shirley background).

sampling the top 4-5 atomic layers (~1.2 nm) to address the question of whether this effect occurs purely on the surface layer of the particles or whether it involves the top several layers of the particles. Comparison of these spectra (see supplementary information)[†] does not show any significant change between probing 2-3 layers and 4-5 layers deep, indicating this is not an effect dominated by a single surface layer.

As the presence of oxygen allows the formation of metal oxide it is also instructive to consider the O 1s spectra in Figure 3, acquired during the same experiment as the Cu and Ni 3p spectra shown in Figure 2 (steps are numbered in both figures). Since some Si 2p signal can be seen (suggesting a nanoparticle coverage of 95%), it should be remembered that some of the oxygen seen originates from the surface oxide layer of the silicon wafer and not from the nanoparticles themselves – and this is likely to be the origin of the peak at around 532.5 eV that remains even in the presence of H_2 at 450 °C. In the presence of O_2 or CO, gas phase peaks (marked in Figure 3) are seen to the higher binding energy side of the 532.5 eV peak as a significant number of gas molecules will inherently be samples (in contrast to an ultra high vacuum experiment).[31] However, the key feature to note is the sudden appearance in O_2 of the lower binding energy features centred at 531.0 and 528.4 eV, which is likely indicative of the formation of metal oxides.[32] Re-examination of the Cu and Ni 3p spectra in Figure 2(b) indicate that only the Cu appears to have been significantly oxidised (inferred from a higher binding energy contribution to the Cu 3p) while the Ni 3p peak width appears unchanged.

CuCo bimetallic nanoparticles

Figure 4(a) shows representative TEM images of the unsupported 11.2 ± 1.4 nm CuCo nanoparticles prepared in an analogous way to the CuNi particles discussed above, along with their corresponding size distribution. Again, STEM-EDS

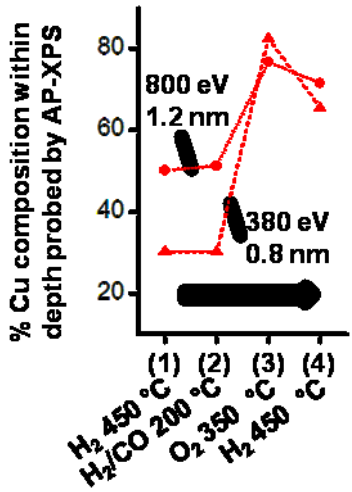

Fig. 6 Relative % of Cu found in surface layers corresponding to 1.2 nm (circles) and 0.8 nm (triangles) mean free paths of escaping electrons during the same series of experiments as shown in Fig. 5, obtained from Cu and Co 3p intensities using incident photon energies of 800 eV and 380 eV respectively (after accounting for the relevant photon energy photoelectron cross sections and the removal of a Shirley background)..

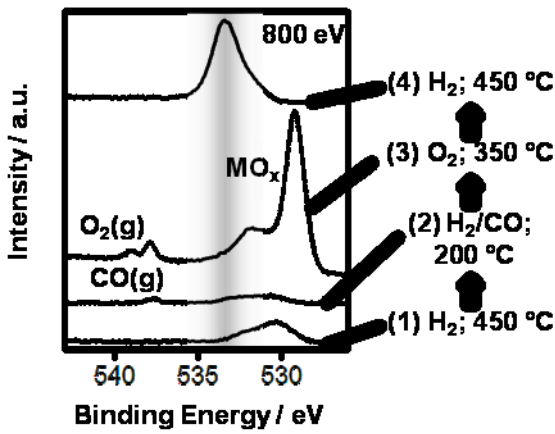

Fig. 7 Ambient pressure O 1s XP Spectra of CuCo nanoparticles supported on the native oxide layer of a silicon wafer during exposure to a series of gases as indicated (0.1 torr) using incident photon energy of 800 eV The data was acquired in the same series of numbered experiments as shown in Fig. 5.

linescans as shown in Figure 4(b) were also acquired to investigate the structure of prepared particles (under the vacuum conditions of the microscope). This time the core-shell type segregation is visibly more marked than in the CuNi case, with the shell nearer the surface appearing to contain most of the cobalt. Overall the expected 1:1 Cu:Co atomic ratio is obtained – for 10 individual particles, on average each

individual particle was found to comprise 55 ± 7 % Cu, in good agreement with the average of 54 % Cu content obtained sampling over a region of many nanoparticles. This is important as it confirms good control of the individual particle compositions, necessary for the interpretation of the AP-XPS spectra that follow – for instance, formation of stray monometallic nanoparticles is unlikely.

As before, these CuCo nanoparticles, after supporting on the oxide surface of a silicon wafer, were then investigated using ambient pressure XPS. Spectra were acquired in vacuum and during the heating steps and introduction of 100 mtorr of H_2 with very little change seen (see supplementary information);[†] the particles initially appear Co rich at the surface, consistent with the large segregation that was seen in the STEM-EDS experiment.[33] The samples were then exposed to a series of reactive gas mixtures (atmospheres ($H_2 \rightarrow$ 1:2 $CO/H_2 \rightarrow O_2 \rightarrow H_2$) and the spectra obtained in the Cu and Co 3p region that correspond to a probing depth of 0.8 nm are shown in Figure 5 (a), along with the calculated surface compositions for each set of conditions. Again, in the presence of oxygen copper is clearly brought to the surface, however the ratio of Cu:Co does not change reversibly back once re-exposed to H_2 and heated to 450 °C. The spectra obtained using different probing depths (Figure 6) indicate that although initially the high surface concentration of Co is likely to be only the very surface layer, the segregation of Cu that occurs in oxygen is a number of layers deep (since spectra probing 1.2 nm and 0.8 nm produce very similar % Cu compositions after exposure to oxygen).

O 1s spectra corresponding to the H_2 and O_2 conditions in the experiment above are shown in Figure 7. As before, there is the sudden appearance of a large low binding energy feature around 529 eV in the presence of oxygen, attributable to metal oxide,[32] which is almost totally removed again on re-exposure to H_2. This time, however, comparison to the spectra in Figures 5 and 6 suggests that both metals are oxidised, as the peaks are shifted to higher binding energy by over 1 eV and have a rounder shape. This latter effect results from the convolution of more than one asymmetric $p_{1/2}$-$p_{3/2}$ doublet (expected intensity ratio of 1:2). For the quality of data acquired from these materials under ambient pressure conditions it is not appropriate to mathematically fit these by de-convolution, however, it is clear by comparison to the asymmetric $p_{1/2}$-$p_{3/2}$ doublet features upon re-exposure to H_2 that these have a significant, higher binding energy contribution – both metals are at least partially oxidised. In contrast to the CuNi case, the CuCo already appears to have a small low binding energy contribution under H_2 before exposure to O_2. This may be the result of stable cobalt oxides being present, which cannot be efficiently reduced under these conditions. There is also a feature remaining on re-exposure to H_2, although from its position (~533 eV) it is likely this may be the result of irreversible further oxidation of the silicon support (in addition to the original native oxide layer), rather than oxidation of the nanoparticles, since the Cu and Co signals appear to indicate limited oxide remains.

Discussion

In the previous section it has been identified that in both cases Cu is segregated to the surface on exposure to O_2. For CuNi the surface returns reversibly to being Ni rich upon exposure to H_2, whereas for CuCo the Cu remains at the surface. In both cases metal oxide formation is observed in oxygen and disappears again on heating in H_2. For CuNi it appears the oxidation occurs predominantly for Cu and not Ni,

whereas for CuCo both metals are oxidised.

It is well known that for bulk materials Cu is expected to surface segregate (in the absence of reactive gases) and has been reported to do so in many experimental studies.[34] This is generally true for both CuCo and CuNi,[34] except at very high Ni contents not relevant to the present study.[35] In the case of bulk alloys (both experimental and theoretical studies have largely been performed on single crystal surfaces), the restructuring is understood for the CuNi case as a balance of cohesive energy (lattice bonding), entropy and surface free energy and surface layer relaxations.[36] Fewer, studies have been performed on CuCo, perhaps because of the large miscibility gap in their phase diagram.[37] In our case copper is never seen to be significantly enriched above the overall bulk composition of 50 % at the surface for the CuNi case, although is enriched further on exposure to oxygen in the case of CuCo. For CuCo it could be argued that heating allowed it to overcome kinetic barriers to diffusion or restructuring, however this occurs on lowering the temperature from 450 to 350 °C ruling out the possibility that the gas is not involved in this transformation. Accordingly, it appears neither case behaves as expected for the bulk materials.

The balance of cohesive energies favours Cu segregation[38] (the higher cohesive energy element being expected to be favourably located in the core, where more bonds with like atoms are possible), but this is not dependant on which gases are present. As outlined in the introduction, for many bimetallic nanoparticles it has been found that they restructure on exposure to reactive gases, such as O_2, as a result of competition between oxide formation enthalpy and surface free energy. However, in here copper has the lowest surface free energy (1.9 Jm^{-2} vs. Co at 2.7 Jm^{-2} and Ni at 2.4 Jm^{-2}) and so in vacuum or H_2 would be expected to be on the surface. For CuCo, in which segregation is mostly confined only to the surface layer, this may explain why Cu remains on the surface after oxygen has caused the segregation to occur. For CuNi, however, it does not explain why nickel segregates to the surface in H_2. It is well known that H_2 can dissociate on nickel surfaces (whereas on copper this requires significant thermal activation). Efficient chemisorption of H_2 is therefore a plausible candidate for this nickel segregation effect, but much more work is needed to fully understand this phenomenon. Similarly, on exposure to oxygen the formation of metal oxides occurs, however this is not to the thermodynamically preferred oxide as seen in previously studied systems ($\Delta H^{\circ}_f\{CuO\} = -157.3$ $kJmol^{-1}$ is significantly less than either $\Delta H^{\circ}_f\{CoO\} = -237.9$ $kJmol^{-1}$ or $\Delta H^{\circ}_f\{NiO\} = -244.4$ $kJmol^{-1}$). This therefore cannot act as the driving force to surface segregate copper – but as it only occurs on exposure to oxygen it seems likely that kinetics or strain effects related to oxide formation must also participate. If kinetics on timescales longer than the ~40 mins of repeat XPS measurements (that suggest stability on this timeframe) are important this could result from diffusion issues or the kinetics of oxide formation and reduction. (In relation to the former, it is interesting to note that interdiffusion in bulk materials is known to be at least 5 times slower for Cu into Ni or CuNi alloys compared to the reverse case of Ni into Cu or CuNi alloys at relevant temperatures.[39]) Given that the oxide formed is in contact with a layer of silicon oxide it is not clear if this interaction is strong enough to also influence the stability of the oxides; it would be very valuable to address this question in future work, but silica was picked for initial use as it is a good mimic for a heterogeneous metal-metal oxide catalyst. Another interesting possibility comes from the case of PtCu in CO gas, which restructures to

give a Cu rich surface alloy on a single crystal both observed experimentally and on the basis of DFT calculations.[40] This is attributed to a uniquely stable surface structure that is preferentially formed in place of the expected strong Pt-CO bonding seen elsewhere, and such effects could also be at work with the copper present in both systems studied here. Another potential issue in addressing the issue of why restructuring can occur in some cases would be the presence of defects or stacking faults altering the kinetics of restructuring – although this doesn't appear to have been reported in the above cases.

Although more detailed investigation is required to understand the nuances of these two systems, *in situ* ambient pressure XPS demonstrates unambiguously the importance of evaluating the surface structure under real reaction conditions in order to understand the surface composition of the actual catalytic surface at work. For instance, although in conditions not directly replicated here, CuNi catalysts for solid oxide fuel cells containing only 10% Ni were still found to cause significant hydrocarbon dissociation (cracking is typically associated with nickel not copper) at temperatures below 800 °C.[41] Although electronic effects have been invoked to explain this involving sub-surface nickel altering the properties of the copper, the present results offer an alternative explanation – nickel rather than copper may be segregated to the surface under the conditions of the reaction. CuNi has also recently been identified by theory and experiment to be an active and highly selective catalyst for methanol synthesis from syngas.[3] Given the strong likelihood of nickel segregation in such catalysts under reducing conditions, their optimisation and development for use as practical catalysts would considerably benefit from an improved understanding of this behaviour. These are just two examples, but given the prevalence of bimetallic catalytic systems, increasing our knowledge of these dramatic restructuring effects is undoubtedly important in understanding their surface chemistry and enabling the rational development of improved catalytic systems.

Conclusions

Bimetallic nanoparticles of 1:1 atomic composition Cu:Ni and Cu:Co (as confirmed by STEM-EDS) and ~11 nm diameter were prepared using a new synthetic method. This has provided two new bimetallic nanoparticle systems, substantially different to those studied previously in the context of surface segregation and restructuring. In vacuum, the as prepared nanoparticles have Ni and Co enriched shells, respectively, and a Cu rich core. Exposure of these nanoparticles supported on planar SiO_2 to a reactive gases results in surface segregation determined *in situ* using ambient pressure XPS. Exposure to O_2 results in a relative increase in the percentage of Cu at the surface as compared to H_2 at 450 °C. For CuNi change is reversible on re-exposure of the nanoparticles to H_2, while the CuCo remains Cu rich at the surface on re-exposure to H_2 at 450 °C. These observations are different to those theoretically and experimentally seen for bulk single crystals in vacuum and clearly not dominated by factors such as surface free energy and the enthalpy of oxide formation as seen in previous studies of bimetallic nanoparticles. Further studies of different sizes and compositions are likely to improve our understanding of the important balance of factors that control these bimetallic systems and others. However, the unexpected results of the present study serve to underline the importance of accounting for these as yet, not fully understood, restructuring effects.

This is especially so for heterogeneous catalysis, where surface composition is crucial and high temperature and pressure reactive gases are usually present.

Table of Contents Graphic

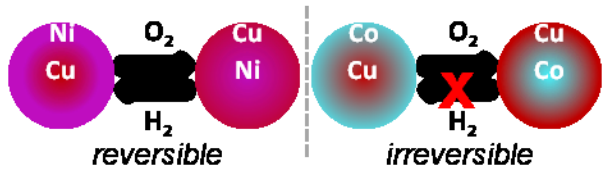

Acknowledgements

GAS acknowledges support from the Director, Office of Sciences, Office of Basic Energy Sciences, Division of Chemical Sciences, Geological and Biosciences of the US Department of Energy (DOE) under contract DE-AC02-05CH11231. NK gratefully acknowledges funding from Total, France. The Advanced Light Source is supported by the Director, Office of Science, Office of Basic Energy Sciences, of the U.S. Department of Energy under Contract No. DE-AC02-05CH11231. The authors are also grateful to Rui Chang at Beamline 9.3.2 for his practical assistance.

[a] *Department of Chemistry, University of California, Berkeley, CA 94720, USA e-mail: somorjai@berkeley.edu*
[b] *Chemical Sciences Division, Lawrence Berkeley National Laboratory, Berkeley, CA 94720, USA*
[c] *Advanced Light Source, Lawrence Berkeley National Laboratory, Berkeley, CA 94720, USA*
[d] *Universite´ Libre de Bruxelles, Campus de la Plaine, CPMPT–CP 243, 50 Av. F. D. Roosevelt, 1050 Bruxelles, Belgium*

† Electronic Supplementary Information (ESI) available: Additional experimental information and SEM characterisation; Additional XPS data. See DOI: 10.1039/b000000x/

‡ Current Addresses: SKB: Durham University, Department of Chemistry, Science Site, South Road, Durham DH3 1LE, UK.; VVP: Dow Corning Corp., 2200 Salzburg Road, Midland, 48686 MI, USA.

References

1 J. A. Rodriguez, in Handbook of Heterogeneous Catalysis, ed. G. Ertl, H. Knözinger, F. Schüth and J. Weitkamp, Wiley-VCH, Weinheim, 2nd edn., 2006, vol. 3, pp. 1298-1309.
2 V. R Calderone, N. R. Shiju, D. Curulla Ferré and G. Rothenberg, *Green Chem*., 2011, **13**, 150.
3 F. Studt, F. Abild-Pedersen, Q. Wuc, A. D. Jensen, B. Temel, J-D. Grunwaldt and J. K. Nørskov, *J. Catal*, 2012, **293**, 51.
4 Y. Chen, F. Yang, Y. Dai, W. Wang and S. Chen *J. Phys. Chem. C* 2008, **112**, 1645.
5 W. M. H. Sachtler, *Faraday Discuss. Chem. Soc.*, 1981, **72,** 7.
6 A. Christensen, A. V. Ruban, P. Stoltze, K. W. Jacobsen, H. L. Skriver and J. K. Nörskov and F. Besenbacher, *Phys. Rev. B*, 1997, **56**, 5822 and refs therein.
7 G. A. Somorjai and Y. Li Introduction to surface chemistry and catalysis, Wiley, Hoboken, 2nd edn., 2010 pp. 296-302.
8 G. Ouyang, C. X. Wang and G. W. Yang, *Chem. Rev.*, 2009, **109**, 4221.
9 J. Y. Park, Y. Zhang, S. H. Joo, Y. Jung and G. A. Somorjai, *Catalysis Today,* 2012, **181**, 133.
10 F. Tao, M. E. Grass, Y. Zhang, D. R. Butcher, F. Aksoy, S. Aloni, V. Altoe, S. Alayoglu, J. R. Renzas, C-K. Tsung, Z. Zhu, Z. Liu, M. Salmeron and G. A. Somorjai, *J. Am. Chem. Soc.*, 2010 **132**, 8697.

11 S. Alayoglu, A. U. Nilekar, M. Mavrikakis and B. Eichhorn, *Nat. Mater.*, 2008, **7**, 333.
12 H. Lang, S. Maldonado, K. J. Stevenson and B. D. Chandler, *J. Am. Chem. Soc.*, 2004, **126**, 12950.
13 F. Tao, S. Zhang, L. Nguyen and X. Zhang, *Chem. Soc. Rev.* 2012, doi: 10.1039/c2cs35185d
14 Assuming hydrogen to be ideal gas colliding with a surface of 10^{15} atoms cm^{-2} at a pressure of 1 torr; D. P. Woodruff and T. A. Delchar. Modern Techniques of Surface Science, Cambridge University Press, Cambridge, 1994.
15 H. Siegbahn, L. Asplund, P. Kelfve, K. Hamrin, L. Karlsson and K. Siegbahn, *J. Electron Spectrosc. Relat. Phenom.*, 1974, **5**, 1059.
16 D.F. Ogletree, H. Bluhm, G. Lebedev, C.S. Fadley, Z. Hussain and M. Salmeron, *Rev. Sci. Instrum.*, 2002, 73, 3872.
17 M. P. Seah and W. A. Dench, *Surf. Interface Anal.*, 1979, **1**, 2.
18 X. Liu, A. Wang, L. Li, T. Zhang, C-Y. Mou, J-F. Lee, *J Catal*, 2011, **278**, 288.
19 S. M. Oxford, P. L. Lee, P. J. Chupas, K. W. Chapman, M. C. Kung, and H. H. Kung, *J. Phys. Chem. C*, 2010, **114**, 17085.
20 S. Alayoglu, F. Tao, V. Altoe, C. Specht, Z. Zhu, F. Aksoy, D. R. Butcher, R. J. Renzas, Z. Liu and G. A. Somorjai, *Catal. Lett.* 2011, **141**, 633.
21 Y. Uemura, Y. Inada, K. K. Bando, T. Sasaki, N. Kamiuchi, K. Eguchi, A. Yagishita, M. Nomura, M. Tada and Y. Iwasawa, *J. Phys. Chem. C*, 2011, **115**, 5823.
22 F. Tao, M. E. Grass, Y. Zhang, D. R. Butcher, J. R. Renzas, Z. Liu, J. Y. Chung, B. S. Mun, M. Salmeron and G A. Somorjai, *Science*, 2008, **322**, 932.
23 K. J. J. Mayrhofer, V. Juhart, K. Hartl, M. Hanzlik and M. Arenz, *Angew. Chemie Int. Ed.*, 2009, 48, 3529.
24 V. Papaefthimiou, T. Dintzer, V. Dupuis, A. Tamion, F. Tournus, D. Teschner, M. Hævecker, A. Knop-Gericke, R. Schlögl and S. Zafeiratos, *J. Phys. Chem. Lett.*, 2010, **2**, 900.
25 S. Alayoglu, S. K. Beaumont, F. Zheng, V. V. Pushkarev, H. Zheng, V. Iablokov, Z. Liu, J. Guo, N. Kruse and G. A. Somorjai, *Top. Catal.*, 2011, **54**, 778.
26 F. Zheng, S. Alayoglu, V. V. Pushkarev, S. K. Beaumont, C. Specht, F. Aksoy, Z. Liu, J. Guo, G. A. Somorjai, *Catal. Today*, 2012, **182**, 54.
27 S. Piccinin, S. Zafeiratos, C. Stampfl, T. W. Hansen, M. Hævecker, D. Teschner, V. I. Bukhtiyarov, F. Girgsdies, A. Knop-Gericke, R. Schlögl, and M. Scheffler, *Phys. Rev. Lett.*, 2010, **104**, 035503.
28 ($\Delta H^{e}_{f}\{CuO\}$ = –157.3 $kJmol^{-1}$; $\Delta H^{e}_{f}\{CoO\}$ = –237.9 $kJmol^{-1}$; $\Delta H^{e}_{f}\{NiO\}$ = –244.4 $kJmol^{-1}$; $\Delta H^{e}_{f}\{Rh_2O_3\}$ = –343 $kJmol^{-1}$, but –172 $kJmol^{-1}$ per Rh atom – taken from David Lide, CRC Handbook of Chemistry and Physics, Taylor and Francis, Raton, 87th edn. 2004).
29 M. E. Grass, P. G. Karlsson, F. Aksoy, M. Lundqvist, B. Wannberg, B. S. Mun, Z. Hussain and Z. Liu, *Rev Sci. Instrum.* 2010, **81**, 053106.
30 J. J. Yeah and I. Lindau, *Atomic Data And Nuclear Data Tables*, 1985, **32**, 55.
31 It should be remembered that it is likely that some nickel carbonyl forms under these conditions and could influence segregation, however $Ni(CO)_4$ is likely to be thermally desorbed if formed; V. Medvedev, R. Börner and N. Kruse, *Surface Sci. Lett.*, 1998, **401**, L371.
32 NIST X-ray Photoelectron Spectroscopy Database, Version 4.1 (National Institute of Standards and Technology, Gaithersburg, 2012); http://srdata.nist.gov/xps/
33 It should be remembered, as mentioned above for CuNi, that prior to heating and the exposure of the sample to reactive gases the cobalt surface enrichment observed may be the result of the preparative procedure / surface contaminants not yet thermally desorbed from the surface. For this reason the data prior to heating in H_2 at 450 °C will not be discussed further but is provided as supplementary information for completeness.
34 N. M. Galea, D. Knapp and T. Ziegler, *J. Catal.*, 2007, **247**, 20.
35 T. Sakurai, T. Hashizume, A. Jimbo, A. Sakai and S. Hyodo, PRL, 1985, **55**, 514.
36 H. Y. Wang, R. Najafabadi, D. J. Srolovitz and R. LeSar, *Phys. Rev. B*, 1992, **45**, 12028.
37 T. Nishizawa and K. Ishida, *Bulletin of Alloy Phase Diagrams*,1984, **5**, 161.
38 Cohesive energies: 3.49 eV per atom of Cu compared to 4.44 eV and 4.39 eV per atom of Ni and Co, respectively; C. Kittel, Introduction to Solid State Physics, John Wiley & Sons, Inc, Hoboken, 8th edn., 2005.

39 D.B. Butrymowicz, J.R. Manning and M.E. Read, *J. Phys. Chem. Ref. Data*, 1976, **5**, 103.
40 K. J. Andersson, F. Calle-Vallejo, J. Rossmeisl and L. Chorkendorff, *J. Am. Chem. Soc.*, 2009, **131**, 2404.
41 H. Kim, C. Lu, W. L. Worrell, J. M. Vohs, and R. J. Gorte, *J. Electrochem. Soc*., 2002, **149**, A247-A250.